Appl. Phys. A (2016) 122:789
DOI 10.1007/s00339-016-0312-4

Applied Physics A
Materials Science & Processing

CrossMark

Photoelectron spectroscopy study of AlN films grown on n-type 6H-SiC by MOCVD

F. Liang[1] · P. Chen[1] · D. G. Zhao[1] · D. S. Jiang[1] · Z. J. Zhao[2] · Z. S. Liu[1] · J. J. Zhu[1] · J. Yang[1] · W. Liu[1] · X. G. He[1] · X. J. Li[1] · X. Li[1] · S. T. Liu[1] · H. Yang[3] · J. P. Liu[3] · L. Q. Zhang[3] · Y. T. Zhang[4] · G. T. Du[4]

Received: 2 March 2016 / Accepted: 26 July 2016 / Published online: 5 August 2016
© Springer-Verlag Berlin Heidelberg 2016

Abstract Photoelectron spectroscopy has been employed to analyze the content and chemical states of the elements on the surface of AlN films with different thickness, which are synthesized by metalorganic chemical vapor deposition on the n-type SiC substrates under low pressure. It is found that, besides the carbon and gallium on the AlN surface, the atom percentage of surface oxygen increases from 4.9 to 8.4, and the electron affinity also increases from 0.36 to 0.97 eV, when the thickness of AlN films increase from 50 to 400 nm. Furthermore, accompanying with the high-resolution XPS spectra of the O 1s, it is speculated that surface oxygen may be the major influence on the electron affinity, where the surface oxygen changes the surface chemical states through replacing N to form Al–O bond and Ga–O bond, although there are also a few of Ga and C contaminations in the chemical sate of Ga–O and C–C, respectively.

✉ P. Chen
pchen@semi.ac.cn

[1] State Key Laboratory on Integrated Optoelectronics, Institute of Semiconductors, Chinese Academy of Science, PO Box 912, Beijing 100083, China

[2] Center for Physicochemical Analysis and Measurement, Institute of Chemistry, Chinese Academy of Sciences, Beijing 100190, China

[3] Suzhou Institute of Nano-tech and Nano-bionics, Chinese Academy of Sciences, Suzhou 215123, China

[4] State Key Laboratory on Integrated Optoelectronics, College of Electronic Science and Engineering, Jilin University, Changchun 130023, China

1 Introduction

As a representative of III-nitrides, AlN is one of the suitable candidates for electronic and optoelectronic applications owing to its unique physical and chemical properties [1, 2], in the fields of UV detectors [3, 4], lasers [5], power electrons [6–8], intersubband transitions for telecommunication [9], surface acoustic waves [10] and hetero-structure field-effect transistors [11, 12]. Especially, since Benjamin [13] suggested a negative electron affinity (NEA) of AlN film through ultraviolet photoelectron spectroscopy (UPS), which was grown on 6H-SiC substrate by molecular beam epitaxy (MBE), the interest in field-emission (FE) applications of AlN film presented a significant rise, even there were some disputations on the value of its electron affinity [14–16]. The materials with NEA can be applied on vacuum microelectronic devices as a cold cathode, such as field-emission displays and micro-vacuum-tubes [14–19], where electrons can be freely extracted from the surface of the cold cathode materials and then escape into the vacuum environment, thus a large field-emission (FE) current and a low turn-on voltage can be obtained.

However, the electron affinity of cathode materials is closely related to the kinds of materials, surface polarity and surface states. Especially, for the AlN film, it is noted that residual impurities is easy to be incorporated during material growth or to form a passive oxide layer while it is exposed into air [20, 21]. In addition, it is reported that oxygen can increase the difficult of doping remarkably and change the Femi level, where the oxygen acts as a compensating defect and introduces deep localized acceptor states (DX centers) [22–24]. On the other hand, X-ray photoelectron spectroscopy (XPS) is an excellent way to characterize the surface feature of semiconductors [24–27] or the interface of alloys [28], by which the content and

chemical states can be investigated directly. In this study, combining the X-ray photoelectron spectroscopy (XPS) measurements with the ultraviolet photoelectron spectroscopy (UPS) analysis, the influence of surface oxygen on the electron affinity has been investigated in detail, and it is assumed that surface oxygen atoms change the surface chemical state by replacing nitrogen atoms to form Al–O bond and Ga–O bond and affect the electron affinity of AlN film.

2 Experimental details

The samples used in this work were Si-doped AlN films with thickness of 50, 200 and 400 nm, which were grown directly on the n-type (001) 6H-SiC substrates at 1100 °C by metalorganic chemical vapor deposition (MOCVD) under a low pressure of 30 Torr. A heterogeneous SiC substrate is preferred to be employed due to two reasons. Firstly, their close lattice constant of about 3.1 Å and thermal expansion coefficients of around 4.2×10^{-6} K^{-1} would benefit to the crystal quality of AlN layers. The second reason is that growing a layer of AlN on a semiconducting (n-type) SiC substrate can lower the difficulty in the XPS and UPS measurement resulted from the poor conductive of AlN material. The precursors of Al, N and Si were trimethylaluminum (TMA), ammonia (NH_3) and SiH_4, respectively. The thickness of the AlN layer is controlled through the growth time, and the AlN samples with thickness of 50, 200 and 400 nm are named as sample A, B and C, respectively. In addition, the Si-doping concentration is semi-quantitatively estimated to be in the order of 10^{18}–10^{19} cm^{-3} according to an uncalibrated second ion mass spectroscopy (SIMS) measurement.

Before carrying out photoelectron spectroscopy measurements, these samples were cut into tablets with size of about 1×1 cm^2 and then surface treatment were taken carefully with acetone, alcohol, deionized water and dilute hydrochloric acid. The tablet of AlN film was mounted on a stainless steel sample holder with a copper clip in an ultra-high-vacuum system while performing the UPS and XPS measurements (ESCALab 250Xi). The content of different elements were obtained by XPS with a monochromatic Al Kα radiation of 1486.6 eV operated at 250 W, whose energy resolution was around 0.6 eV, and the base pressure in the chamber was about 2×10^{-9} mbar. The binding energies were calibrated by referencing the C 1s core line at 284.8 eV of the hydrocarbon. Meanwhile, when taking UPS measurement, a helium gas discharge lamp was employed as the ultraviolet light source and the helium pressure in the chamber was about 2×10^{-8} mbar. In addition, the electron affinity (χ) of AlN samples can be determined through UPS spectrum as following expression:

$$\chi = h\nu - W - E_g \quad (1)$$

where $h\nu$, W and E_g are the photon energy (He I, 21.2 eV), width of UPS spectrum and band gap of AlN (6.2 eV), respectively. Here, the width W is derived from the onset of the low kinetic energy limit to the end of the high kinetic energy limit in the UPS spectrum, corresponding to the energy of inelastic secondary electron cutoff ($E_{\text{cut-off}}$) and the valence band maximum (E_{VBM}), respectively.

3 Results and discussion

XPS survey scans were employed firstly to analysis the elemental composition, before taking UPS measurement. As shown in Fig. 1, the results of the XPS survey of Sample A, B and C reveal that the surface of these three AlN samples are composed of the Ga, Al, C, N and O. However, the XPS spectra could not reveal Si dopant, because there was a strong interference between the Si 2p peak and the energy loss peak of Al, and also the amount of Si dopant is much lower compared with the content of Al. In addition, the AlN samples may also contain hydrogen; however, it cannot be detected by XPS because of its small atomic number value and small photo-ionization cross section. High-resolution narrow scans of Ga 3d, Al 2p, C 1s, N 1s and O 1s peaks were taken to obtain their content, and the results are shown in Table 1, and the content of different elements are expressed by the values of atom percentage.

For Sample A, besides the Al and N, with high atom percentage of 41.8 and 33.6, respectively, there are also Ga, O and C on its surface, with atom percentages of 2,

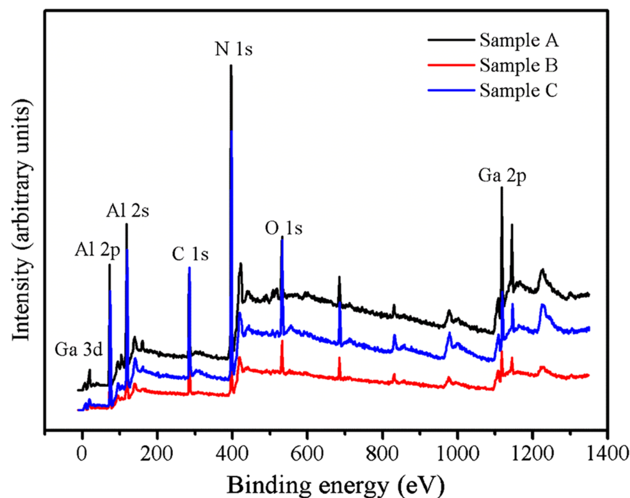

Fig. 1 XPS survey spectra of AlN films

Table 1 XPS quantification of elemental composition on AlN film surface

Sample	A	B	C
Atomic percentage (%)			
Ga	2	1.2	0.9
Al	41.8	41.1	39.6
C	17.7	13.9	22.5
N	33.6	38.4	28.6
O	4.9	5.4	8.4

17.7 and 4.9, respectively. For the Sample B, in addition to the Al of 41.1 % and N of 38.4 %, Ga, O and C also exist on its surface, with atom percentages of 1.2, 13.9 and 5.4, respectively. Meanwhile, for Sample C, in addition to the Al of 39.6 % and N of 28.6 %, Ga, O and C also exist on its surface, with atom percentages of 0.9, 22.5 and 8.4, respectively.

It is noted that the surface oxygen may come from two sources, i.e., surface oxidation and incorporation during growing. First, due to its readily oxidizable character, surface oxidation of AlN material is a frequent occurrence indeed [20, 21]. On the other hand, oxygen may also be induced during growth proved by Kakanakova-Georgieva [24] and Kuech [25]. In brief, they demonstrated that the incorporation of oxygen in Al-containing alloys, such as AlGaN and AlGaAs crystallinity, were attributed to the ready reaction between the trimethylaluminum precursor and oxygen in the gas stream where $Al(CH_3)_2CH_3OH$ product can be formed.

It is also observed that there is always Ga for these three AlN samples. In the research of properties of the InAlN layers grown by MOCVD, Kim [29], Choi [30] and Zhou [31] reported that the Ga contamination should result from the inter-diffusion among reactor walls, susceptor and/or showerhead. Thus, in a similar way, it is suspected that the Ga impurity is more likely to be introduced into the samples due to its high growth temperature of 1100 °C and the incompletely clean vacuum chamber of the MOCVD system, where Ga could become a residual impurity after GaN or GaAs film growth in the same system. On the other hand, we suspect that Ga impurity may comes from the incompletely clean vacuum chamber of our MOCVD system, in which Ga may become a residual impurity after GaN or GaAs film growth in the same system. In addition, the atom percentage of C on the AlN surface is much larger than that of Ga and O, which will be explained further in the following text.

To investigate the influence of surface impurities on the electron affinity of these three AlN samples, the UPS analysis was taken to obtain the electron affinity. A −10 V bias was employed when taking the UPS measurements, which can avoid the spectrometer's work function effect and make the UPS spectra structure clearer. It is noted that

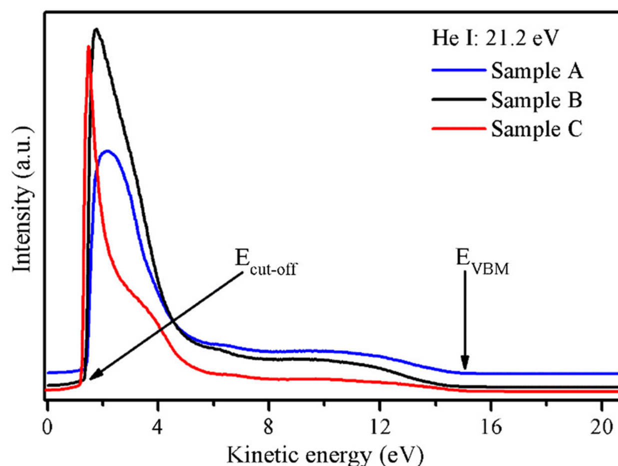

Fig. 2 UV photoemission spectra of AlN films

these UPS spectra present an intense and narrow emission peak at the low kinetic energy end of photoemission spectra, which was also found by Weide et al. [32, 33] when they studied the electron affinity of C (1000) and was assigned to the negative electron affinity (NEA). Then, Wu and Kahn [15] reported that this peak was owing to the huge secondary electrons thermalized to conduction band minimum at the surface instead of NEA.

For our samples, all the values of the electron affinity is obtained through Eq. (1), and the width W of the UPS spectra in Fig. 2 was obtained first by using a linear extrapolation to determine the inelastic secondary electron cutoff ($E_{\text{cut-off}}$) and the valence band maximum (E_{VBM}), which is marked with arrow in the UPS spectra. Then, combining with the band gap (E_g) of AlN as 6.2 eV and the photon energy (hv) of 21.2 eV, the electron affinity (χ) was obtained through the Eq. (1), which is 0.36, 0.58, 0.97 eV for Sample A, B and C, respectively. It is noted that the electron affinity for our AlN simples is positive and the value of the electron affinity shows an increase with thickness increasing.

For the band gap (E_g) of AlN, Motamedi and Cadien [34] proposed that the optical band gap of AlN film depends on the film thickness, when they investigated the structural and optical characterization of low-temperature ALD (atomic layer deposition) crystalline AlN. On one side, the band gap increases as the thickness increases from 4 to 16 nm. Meanwhile, it is also demonstrated that, for a wider range of thicknesses, i.e., more than 15 nm, the value of the band gap levels off at the bulk value with a range of 0.04 eV. For our samples used in this manuscript, the film thickness is more than 50 nm, and the difference of the electron affinity is in the order of 0.2 eV. Thus, it is suggested that the influence of the thickness on the band gap of our AlN samples may be slightly and the value of electron affinity should be reliable.

As shown in Fig. 3 in detail, the value of electron affinity, i.e., 0.36, 0.58 and 0.97 eV, and the atom percentage of surface oxygen, i.e., 4.9, 5.4 and 8.4 % for the 50, 200 and 400 nm-thick AlN samples, respectively, show an increase with increasing thickness. It is reported that an exposure of GaN material to O_2 was sufficient to remove the surface states near the band edges, which could lead to an increase for electron affinity [35]. In addition, Wu et al. [36] demonstrated that the surface O would lead to a bend upward for the conduction band of α-Fe_2O_3 nanoflakes and then an increase of the surface work function. To some degree, it is speculated that the increase of surface O contamination may have an influence on the electron affinity. Therefore, the high-resolution XPS spectra of O, Ga and C were taken to investigate surface chemical state.

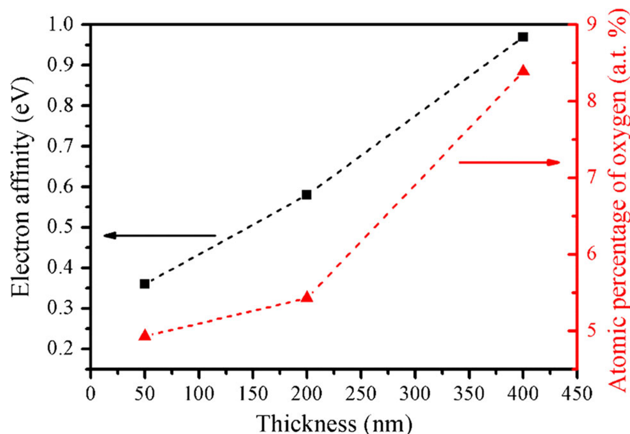

Fig. 3 Electron affinity and content of surface O for sample A, B and C

Figure 4a shows that the main peaks of O 1s are almost located at near 532 eV, which could be decomposed with three sub-peaks, i.e., three chemical states. In detail, in Fig. 4b, for Sample A, the spectrum of O 1s can be fitted at binding energies of 530.76, 531.83 and 532.82 eV. In Fig. 4c, for Sample B, it can be fitted with three sub-peaks at binding energies of 530.23, 531.61 and 532.62 eV. In Fig. 4d, for Sample C, the O 1s core level can be also

Fig. 4 High-resolution XPS spectra of the O 1s for Sample A, B and C. All the *red dash lines*, *triangle-lines*, *black solid squares* and *black solid lines* are the fitting curves, decomposed curves (i.e. sub-peaks), original XPS data and background data, respectively

Table 2 Atomic percentage of O and Ga in different chemical states

Sample	A	B	C
Atomic percentage (at.%)			
O			
Ga–O	16.4	7.9	17.1
Al–O	40.2	51.2	44.8
C–O	43.4	40.9	38.1
Ga			
Ga–Ga	37.2	57.6	53.7
Ga–O	62.8	42.4	46.3
O			
C–C	98.4	96.1	98.7
C–O	1.6	3.9	1.3

decomposed at binding energies of 530.51, 531.72 and 532.73 eV. In summary, the sub-peaks around 530.6, 531.8 and 532.8 eV are assigned to Ga–O bond [37, 38], Al–O bond [39, 40] and C–O bond, respectively, which indicates that most of O atoms replace the N and bind with Al or Ga in Al–O or Ga–O bond. The atomic percentage of these three chemical states is shown in Table 2. It demonstrates that the chemical states of AlN surface has been changed by the surface O contamination. Benjamin et al. [13] reported that the surface O may affect the surface structure and termination of the AlN and then lead to a change of the electron affinity related features in UPS spectra. Meanwhile, Martin et al. [41, 42] had also demonstrated that oxygen contamination at their samples might have an influence on the electron affinity, where the absorbed oxygen is found to increase the ionization energy and thus change the electron affinity of AlN and AlGaN. Therefore, for our three AlN samples, the electron affinity may be mainly influenced by the surface oxygen, which change the surface composition and chemical state through forming into Al–O bond and Ga–O bond, where the electron affinity shows an increase when the amount of oxygen increasing.

Besides the oxygen, the chemical state of Ga is also explored. In Fig. 5a, the high-resolution XPS spectra of the Ga 3d indicate that there may be different chemical states.

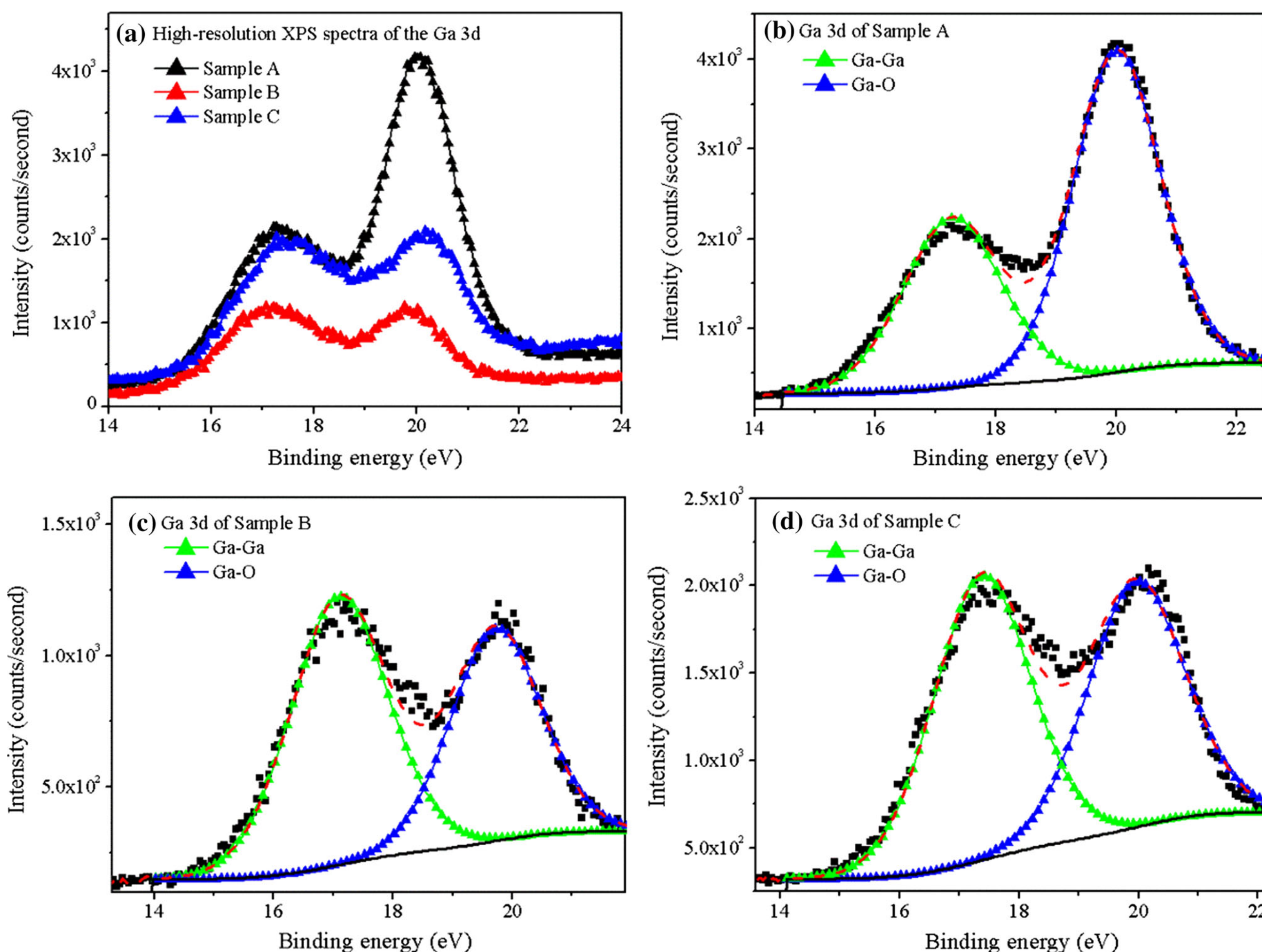

Fig. 5 High-resolution XPS spectra of the Ga 3d for Sample A, B and C. All the *red dash lines*, *triangle-lines*, *black solid squares* and *black solid lines* are the fitting curves, decomposed curves (i.e. sub-peaks), original XPS data and background data, respectively

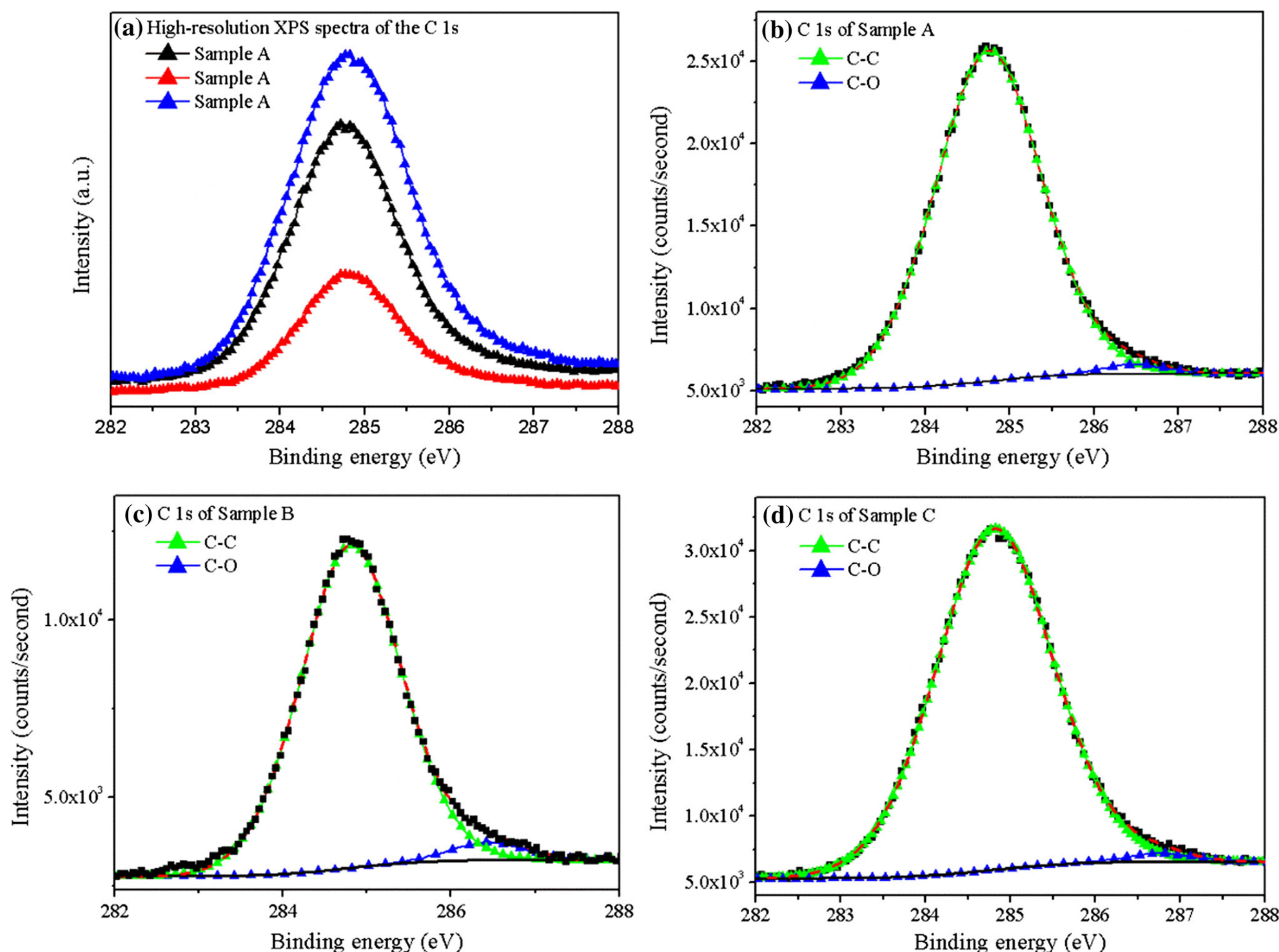

Fig. 6 High-resolution XPS spectra of the C 1s for Sample A, B and C. All the *red dash lines*, *triangle-lines*, *black solid squares* and *black solid lines* are the fitting curves, decomposed curves (i.e. sub-peaks), original XPS data and background data, respectively

In Fig. 5b, for Sample A, the Ga 3d spectrum can be fitted with two sub-peaks at the binding energies of 17.28 and 20.01 eV, respectively. In Fig. 5c, for Sample B, it also can be decomposed with two sub-peaks at the binding energies of 17.1 and 19.72 eV, respectively. In Fig. 5d, for Sample C, it can be decomposed with two sub-peaks at the binding energies of 17.38 and 19.96 eV, respectively. In Fig. 5b–d, the chemical states at the binding energy of around 17 eV and about 20 eV are assigned to Ga–Ga band [43] and Ga–O bond [44], respectively. All the atomic percentage of these chemical states is shown in Table 2. However, compared with the amount of oxygen, the content of Ga is much less. In addition, as a third group element, Ga should be less significant to change the electron affinity. Thus, for our three AlN samples, the main effect on the electron affinity is possible from the surface oxygen.

As shown in Table 1, in addition to O and Ga, there is always C on the AlN surface and its content is much larger than that of Ga and O. As displayed in Fig. 6a, the high-resolution XPS spectra of the C 1s are employed to analyze its chemical states. In Fig. 6b, for sample A, C 1s spectrum can be fitted with two sub-peaks at the binding energies of 284.75 and 286.46 eV, respectively. In Fig. 6b, for sample B, it can be fitted with two sub-peaks at the binding energies of 284.81 and 286.43 eV, respectively. In Fig. 6d, for sample C, it can be also fitted with two sub-peaks at the binding energies of 284.81 and 286.74 eV, respectively. In addition, the atomic percentage of these chemical states is shown in Table 2. It is noted that there may be incorporated during the MOCVD growth or introduced by surface treatment. If C is incorporated during the period of AlN growth, it would mainly substitute for N to form C_N defect [45, 46]. However, for our three AlN samples, most of C with the binding energy of near 284.8 eV is in C–C chemical state, meanwhile, and a few of C with the binding energy of 286.5 eV is attributed to the C–O bond of the hydrocarbon. It is suggested that the C should be assigned to the surface contamination, like acetone or alcohol treatment, in which chemical states of C–C bond or C–O bond is more possible to be exist rather that the C_N defect.

Therefore, compared with surface oxygen, which replaces N to form into Al–O and Ga–O bond, the surface C maybe has less influence on the electron affinity.

4 Conclusions

XPS and UPS analysis has been taken to research the AlN surface and its influence on the electron affinity of the Si-doped AlN films with different thickness, which are grown by MOCVD under low pressure on the n-type SiC substrates. It reveals that the atom percentage of surface oxygen and the electron affinity increase, when the thickness increase from 50 to 400 nm. Furthermore, accompanying with the high-resolution spectra of the O 1s, it is surmised that surface oxygen may be the major influence on the electron affinity, although there are also a few of Ga and C contaminations on the AlN surface.

Acknowledgments The authors acknowledge the support from the National Natural Science Foundation of China (Grant Nos. 61574135, 61574134, 61474142, 61474110, 61377020, 61376089, 61223005, and 61321063), One Hundred Person Project of the Chinese Academy of Sciences, and Basic Research Project of Jiangsu Province (Grant No. BK20130362).

References

1. Y.B. Tang, H.T. Cong, Z.M. Wang, H.M. Cheng, Appl. Phys. Lett. **89**, 253112 (2006)
2. K. Asghar, D. Das, J. Semicond. **37**, 036001 (2016)
3. E. Cicek, R. McClintock, C.Y. Cho, B. Rahnema, M. Razeghi, Appl. Phys. Lett. **103**, 181113 (2013)
4. M. Yang, M. Chong, D.G. Zhao et al., J. Semicond. **35**, 064008 (2014)
5. M. Martens, F. Mehnke, C. Kuhn et al., IEEE Photonics Technol. Lett. **26**, 342 (2014)
6. X.B. Song, G.D. Gu, Y.G. Wang et al., J. Semicond. **37**, 044007 (2016)
7. M.H. Wong, Y. Pei, J.S. Speck, U.K. Mishra, Appl. Phys. Lett. **94**, 182103 (2009)
8. Y.H. Chen, X.F. Zheng, J.C. Zhang et al., J. Semicond. **37**, 055002 (2016)
9. D. Hofstetter, E. Baumann, F.R. Giorgetta et al., Proc. IEEE **98**, 1234 (2010)
10. C.M. Lin, Y.Y. Yu, V.V. Felmetsger et al., J. Micromech. Microeng. **23**, 025019 (2013)
11. J.T. Zhao, Z.J. Lin, C.B. Luan et al., J. Semicond. **35**, 124003 (2014)
12. Y.X. Yu, Z.J. Lin, Y.J. Lv et al., J. Semicond. **35**, 124007 (2014)
13. M.C. Benjamin, C. Wang, R.F. Davis, R.J. Nemanich, Appl. Phys. Lett. **64**, 3288 (1994)
14. C.I. Wu, A. Kahn, E.S. Hellman, D.N.E. Buchanan, Appl. Phys. Lett. **73**, 1346 (1998)
15. C.I. Wu, A. Kahn, Appl. Phys. Lett. **74**, 546 (1999)
16. C.I. Wu, A. Kahn, Appl. Phys. Lett. **74**, 1433 (1999)
17. A.T. Sowers, J.A. Christman, M.D. Bremser et al., Appl. Phys. Lett. **71**, 2289 (1997)
18. Y. Taniyasu, M. Kasu, T. Makimoto, N. Kobayashi, Phys. Status Solidi A **200**, 199 (2003)
19. Y. Taniyasu, M. Kasu, T. Makimoto, Appl. Phys. Lett. **84**, 2115 (2004)
20. S.W. King, J.P. Barnak, M.D. Bremser et al., J. Appl. Phys. **84**, 5248 (1998)
21. D. Chen, D. Xu, J.J. Wang, Y.F. Zhang, J. Phys. D Appl. Phys. **41**, 235303 (2008)
22. T. Mattila, R.M. Nieminen, Phys. Rev. B **54**, 16676 (1996)
23. L. Silvestri, K. Dunn, S. Prawer, F. Ladouceur, Appl. Phys. Lett. **99**, 122109 (2011)
24. A. Kakanakova-Georgieva, D. Nilsson, X.T. Trinh, Appl. Phys. Lett. **102**, 132113 (2013)
25. T.F. Kuech, D.J. Wolford, E. Veuhoff, V. Deline, J. Appl. Phys. **62**, 632 (1987)
26. P. Motamedi, K. Cadien, Appl. Surf. Sci. **315**, 104 (2014)
27. F.L.M. Khir, M. Myers, A. Podolska, Appl. Surf. Sci. **314**, 850 (2014)
28. C. Han, Y.M. Zhang, Q.W. Song et al., J. Semicond. **36**, 123006 (2015)
29. J. Kim, Z. Lochner, M.H. Ji et al., J. Cryst. Growth **388**, 143 (2014)
30. S. Choi, H.J. Kim, Z. Lochner et al., J. Cryst. Growth **388**, 137 (2014)
31. K. Zhou, M. Ikeda, J.P. Liu et al., J. Cryst. Growth **409**, 51 (2015)
32. J. van der Weide, R.J. Nemanich, J. Vac. Sci. Technol. B **10**, 1940 (1992)
33. J. van der Weide, Z. Zhang, P.K. Baumann, Phys. Rev. B **50**, 5803 (1994)
34. P. Motamedi, K. Cadien, J. Cryst. Growth **421**, 45 (2015)
35. V.M. Bermudez, J. Appl. Phys. **80**, 1190 (1996)
36. J.Q. Wu, S.Z. Deng, N.S. Xu, J. Chen, Appl. Surf. Sci. **292**, 454 (2014)
37. G. Schön, J. Electron Spectrosc. **2**, 75 (1973)
38. W. Wei, Z.X. Qin, S.F. Fan et al., Nanoscale Res. Lett. **7**, 562 (2012)
39. E. Paparazzo, Surf. Interface Anal. **12**, 115 (1988)
40. P. Motamedi, K. Cadien, Appl. Surf. Sci. **315**, 104 (2014)
41. G. Martin, S. Strite, A. Botchkarev, Appl. Phys. Lett. **65**, 610 (1994)
42. G. Martin, A. Botchkarev, A. Rockett, Appl. Phys. Lett. **68**, 2541 (1996)
43. M. Kumar, A. Kumar, S.B. Thapa, Mater. Sci. Eng. B **186**, 89 (2014)
44. D. Sadowska, A. Gladki, K. Mazur, E. Talik, Vacuum **72**, 217 (2004)
45. J.L. Lyons, A. Janotti, C.G. Van de Walle, Appl. Phys. Lett. **97**, 152108 (2010)
46. M.A. Reshchikov, H. Morkoç, J. Appl. Phys. **97**, 061301 (2005)